

Differences in Stability, Cytotoxicity, and Mechanism of Action of Ru(II) and Pt(II) Complexes of a Bidentate N,O Donor Ligand

Moumita Maji, Sourav Acharya, Saptarshi Maji, Kallol Purkait, Arnab Gupta, and Arindam Mukherjee*

Cite This: <https://dx.doi.org/10.1021/acs.inorgchem.0c01433>

Read Online

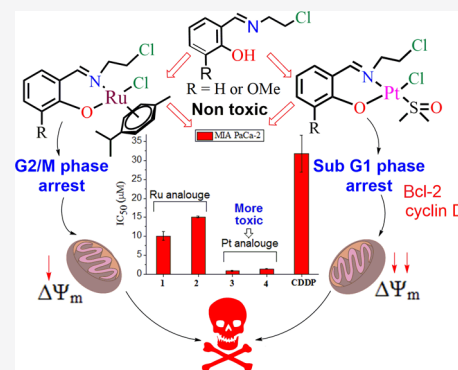
ACCESS |

Metrics & More

Article Recommendations

Supporting Information

ABSTRACT: We report $[\text{Ru}^{\text{II}}(\text{L})(\eta^6\text{-}p\text{-cym})\text{Cl}]$ (**1** and **2**) and $[\text{Pt}^{\text{II}}(\text{L})(\text{DMSO})\text{Cl}]$ (**3** and **4**) complexes, where L is a chelate imine ligand derived from chloroethylamine and salicylaldehyde (HL1) or o-vanillin (HL2). The complexes were characterized by single-crystal X-ray diffraction and other analytical techniques. The ^1H nuclear magnetic resonance data show that both the Ru(II) and Pt(II) complexes start forming the aquated complex within an hour. The aquated complexes are stable at least up to 24 h. The complexes bind to the N^7 of the model nucleobase 9-ethylguanine (9-EtG). Interaction with calf thymus (CT) DNA shows moderate binding interactions with binding constants, K_b , $(3.7 \pm 1.2) \times 10^3 \text{ M}^{-1}$ and $(4.3 \pm 1.9) \times 10^3 \text{ M}^{-1}$ for **1** and **3**, respectively. The complexes exhibit significant antiproliferative activity against human pancreas ductal adenocarcinoma (Mia PaCa-2), triple negative metastatic breast adenocarcinoma (MDA-MB-231), hepatocellular carcinoma (Hep G2), and colorectal adenocarcinoma (HT-29) cell lines. The studies show that with the same ligand the Pt(II) complexes are more potent than the Ru(II) complexes. The *in vitro* potencies of all the complexes toward pancreatic cancer cell line Mia PaCa-2 are more than cisplatin (CDDP). The Pt(II) and Ru(II) complexes show similar binding constants with CT-DNA, but the reactivity of the Pt(II) complex **3** with 9-EtG is faster and their overall cell killing pathways are different. This is evident from the arrest of the cell cycle by the Ru(II) complex **1** in the G2/M phase in contrast to the SubG1 phase arrest by the Pt(II) complex **3**. The immunoblot study shows that **3** increases cyclin D and Bcl-2 expression in MDA-MB-231 due to the SubG1 phase arrest where these proteins express in greater quantities. However, both **1** and **3** kill in the apoptotic pathway via dose-dependent activation of caspase 3. Complex **3** depolarizes the mitochondria more efficiently than **1**, suggesting its higher preference for the intrinsic pathway of apoptosis. Our work reveals that the same bidentate ligand with a change of the metal center, *viz.* Pt(II) or Ru(II), imparts significant variation in cytotoxic dosage and pathway of action due to specific intrinsic properties of a metal center (*viz.* coordination geometry, solution stability) manifested in a complex.



INTRODUCTION

The Pt drugs hold strong ground in cancer chemotherapy^{1–3} with at least six of them in the clinic worldwide, including the three FDA approved ones (cisplatin, carboplatin, and oxaliplatin).⁴ A primary mechanism of cytotoxicity of Pt(II) complexes is by cross-linking DNA.^{5,6} This cross-linking leads to the deformation of the DNA structure, which hinders the replication and transcription of DNA leading to cell cycle arrest and apoptosis.⁴ However, the resistance to the existing Pt drugs creates a demand for newer anticancer agents with better toxicity.^{7,8} Among the various strategies to elevate the toxicity toward multiple cancers, one is the combination with other active drugs or motifs to generate new cytotoxic metal complexes.^{7,9–14} The change of metal from Pt to Ru attracts much attention owing to the ability to act against Pt-resistant cancers and exhibit lesser side effects.^{15,16} Several Ru(III) complexes, *viz.* NAMI-A and NKP1339, have undergone clinical trials.^{17–19} TLD-1433 is the first example of a Ru(II) complex that entered phase-I clinical trials as a photodynamic therapy (PDT) agent against BCG refractory high-risk

nonmuscle invasive bladder cancer.²⁰ Several Ru(II) half-sandwich complexes, *viz.* RM-175 and RAPTA-C, have shown promising activity in preclinical trials.^{21–23} The anticancer activity, stability, and mechanism of action of these complexes can be tuned by the appropriate choice of attached ligand, arene, and halides.^{24–26}

We have earlier shown that Pt(II) complexes of nitrogen mustards increase the stability of the mustard ligands and render complexes with improved activity.^{7,9,10} The bis(2-chloroethylamine) motif of the nitrogen mustard drug is responsible for the DNA alkylation.^{7,9,10} The nitrogen mustard drug cyclophosphamide and its analogue ifosfamide were

Received: May 15, 2020

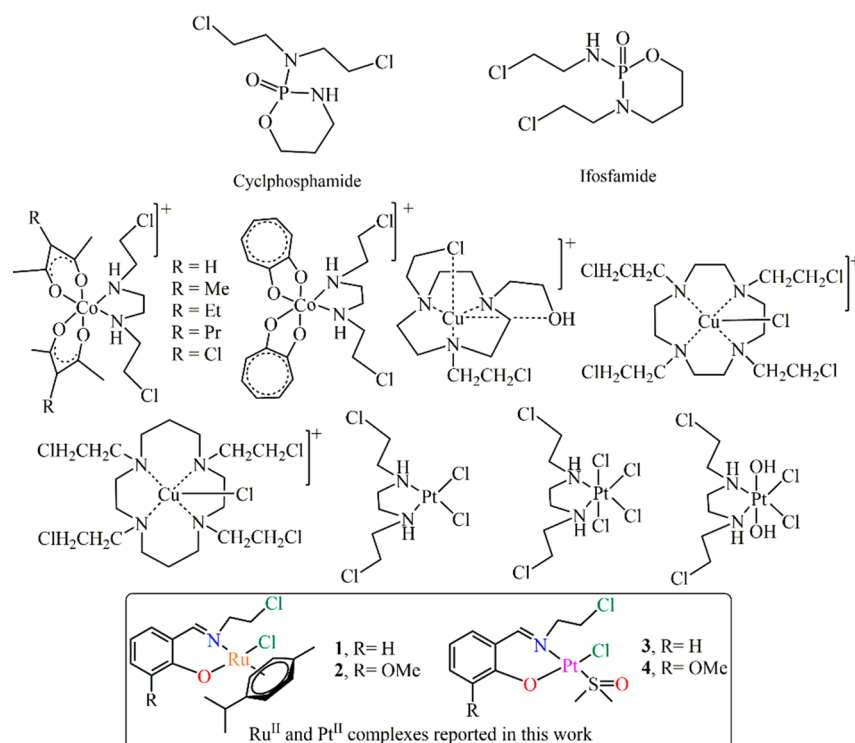


Figure 1. Reported metal complexes conjugated with chloroethylamine and representation of metal complexes in the current work.^{27–29}

approved by the FDA in 1959 and 1987, respectively (Figure 1). The bis(2-chloroethylamine) motif in cyclophosphamide is replaced by a chloroethylamine motif in ifosfamide, which also acts as a DNA alkylating motif, albeit rather slowly. Both ifosfamide and cyclophosphamide require metabolic activation to exert their anticancer activity. In the recent past, cyclophosphamide has been approved for oral use too. Thus, our ongoing efforts are to investigate the effect of the chloroethylamine motif as part of a ligand where the N atom coordinates to the metal center and the chloro substituent in the aliphatic chain remains pendant. The complexes of Co^{III} and Cu^{II} with chloroethylamine motifs are very active against certain cancers and exhibit activation upon reduction in hypoxia (Figure 1).^{27,28} The aim of the present study is to investigate the effect of the variation of the metal center between Ru(II) and Pt(II), by keeping the same chloroethylamine motif bearing ligand(s), since Pt(II) complexes containing this particular moiety are scarce^{27–29} and Ru(II) complexes of the same are not known. However, Pt(II) or Ru(II)-*p*-cymene complexes of various other salicylaldehyde based ligands have shown anticancer activity, stabilization of telomeres, and efficiency in catalysis.^{30–35} In addition, earlier works show that using one ligand and varying the metal center (Ir, Ru, or Rh) has a substantial impact on the solution stability and also alters the cytotoxicity of a resultant complex against a particular type of cancer.^{36–39}

The work presented here involves two Ru(II) (1 and 2) and two Pt(II) (3 and 4) complexes of two bidentate ligands. The ligands were synthesized from chloroethylamine by a condensation reaction with salicylaldehyde (HL1) or *o*-vanillin (HL2) to form bidentate chelating Schiff bases. The complexes are compared for their stability studies in aqueous media, binding to DNA and cytotoxicity against four aggressive human cancer cell lines: pancreas ductal adenocarcinoma (Mia PaCa-2), triple negative metastatic breast adenocarcinoma

(MDA-MB-231), hepatocellular carcinoma (HepG2), and colorectal adenocarcinoma (HT-29) cell lines.

EXPERIMENTAL SECTION

Materials and Methods. All the chemicals were purchased from commercial sources and used without any further purification. The solvents were distilled by standard procedures, prior to use. The metal precursor complexes [Ru^{II}₂(η^6 -*p*-cym)₂(Cl)₄] and [Pt(DMSO)₂Cl₂] were synthesized following the literature procedures.^{40,41} MTT [(3-(4,5-dimethylthiazol-2-yl)-2,5-diphenyltetrazolium bromide)] (USB) and other supplements were purchased from Gibco and used as received. 9-Ethyl guanine (9-EtG) was purchased from Sigma-Aldrich. The solvents used for spectroscopic measurements were of spectroscopy grade and purchased from Merck, India. UV–visible experiments were performed using Agilent Technologies Cary 300 Bio. The FT-IR spectra were recorded using a PerkinElmer SPECTRUM RX I spectrometer in KBr pellets. The ¹H NMR, ¹³C{¹H} NMR, and HMQC spectra were recorded using either a 400 MHz JEOL ECS or 500 MHz Bruker Avance III spectrometer, at room temperature (24–27 °C). The chemical shifts of the relevant compounds are reported in parts per million (ppm). All the mass spectra (ESI-MS) were recorded in positive mode electrospray ionization using a Bruker maxis II instrument. Isolated yields of ¹H NMR pure compounds are reported.

Syntheses. *Synthesis of (E)-2-(((2-chloroethyl)imino)methyl)phenol (HL1).* This compound was synthesized by following a literature procedure.⁴² Briefly, salicylaldehyde (5 mmol) and 2-chloroethylamine hydrochloride (5 mmol) were taken in ethanol; 5 mmol of NaOH was dissolved in 5 mL of water and added to the above solution. This reaction mixture was heated to reflux for 6 h. After cooling to 25 °C, the reaction mixture was added to 40 mL of water in an ice bath and kept for 30 min. Yellow crystals formed, which were filtered off and washed with slightly cold water and dried in a vacuum. Yield: 76%. ¹H NMR (CDCl₃, 500 MHz, 298 K): δ (ppm): 13.0 (s, 1H, O–H), 8.38 (s, 1H, H–C=N), 7.33 (t, 1H, *J* = 8.0 Hz, phenyl–H), 7.27 (d, 1H, *J* = 7.5 Hz, phenyl–H), 6.98 (d, 1H, *J* = 8.5 Hz, phenyl–H), 6.89 (t, 1H, *J* = 7.5 Hz, phenyl–H), 3.91 (t, 2H, *J*₁ = 5.5 Hz, *J*₂ = 6.0 Hz, N–CH₂–), 3.80 (t, 2H, *J*₁ = 5.0 Hz, *J*₂ = 6.0 Hz, N–CH₂–).

6.5 Hz, $-\text{CH}_2\text{Cl}$) (Figure S1). $^{13}\text{C}\{^1\text{H}\}$ NMR (CDCl_3 , 125 MHz, 298 K) δ (ppm): 167.1, 160.9, 132.6, 131.6, 118.7, 118.4, 117.0, 60.7, 43.8 (Figure S2).

Synthesis of (E)-2-(((2-chloroethyl)imino)methyl)-6-methoxyphenol (HL2). HL2 was prepared by a similar procedure to that discussed above for HL1. Yield: 80%. ^1H NMR (CDCl_3 , 500 MHz, 298 K): δ (ppm) 8.38 (s, 1H, $\text{H}-\text{C}=\text{N}$), 6.96 (d, 1H, $J = 8.0$ Hz, phenyl-H), 6.92 (d, 1H, $J = 7.5$ Hz, phenyl-H), 6.83 (t, 1H, $J_1 = 8$ Hz, $J_2 = 7.5$ Hz, phenyl-H), 3.92 (t, 2H, $J_1 = 6.5$ Hz, $J_2 = 7.5$ Hz, $\text{N}-\text{CH}_2-$), 3.90 (s, 1H, $-\text{OCH}_3$), 3.79 (t, 2H, $J_1 = 6.0$ Hz, $J_2 = 5.5$ Hz, $-\text{CH}_2\text{Cl}$; Figure S3). $^{13}\text{C}\{^1\text{H}\}$ NMR (CDCl_3 , 125 MHz, 298 K): δ (ppm) 167.1, 151.2, 148.3, 123.1, 118.3, 118.1, 114.3, 60.4, 56.0, 43.8 (Figure S4).

General Procedure for Preparation of Ru^{II} Complexes (1 and 2). The complexes were synthesized according to a procedure similar to that reported by us earlier.³³ Precisely, to a 10 mL methanolic solution the respective ligands (0.1 mmol), KOH (0.1 mmol) were added and stirred for 15 min at 25 °C. Then, 15 mL of a methanolic solution of $[\text{Ru}^{\text{II}}_2(\eta^6\text{-p-cym})_2(\text{Cl})_4]$ (0.05 mmol) was added in the dark under a nitrogen atmosphere at 25 °C. The reaction mixture was stirred at 25 °C for 12 h followed by evaporation. An orange mass was isolated, which was dissolved in DCM, and any solid was filtered off. The filtrate was evaporated and washed with diethyl ether.

$[\text{Ru}^{\text{II}}(\text{L1})(\eta^6\text{-p-cym})\text{Cl}]$ (1). Yield: 65%. ^1H NMR (CDCl_3 , 500 MHz, 298 K): δ (ppm) 7.76 (s, 1H, $\text{H}-\text{C}=\text{N}$), 7.23 (td, 1H, $J_1 = 8.5$ Hz, $J_2 = 1.5$ Hz, phenyl-H), 6.97 (t, 2H, $J = 8.5$ Hz, phenyl-H), 6.46 (t, 1H, $J = 8.0$ Hz, phenyl-H), 5.47 (m, 3H, $p\text{-cym-H}$), 5.11 (d, 1H, $J = 5.5$ Hz, $p\text{-cym-H}$), 4.55 (m, 1H, $\text{N}-\text{CH}_2-$), 4.37 (m, 2H, $-\text{CH}_2\text{Cl}$), 3.88 (m, 1H, $\text{N}-\text{CH}_2-$), 2.83 (m, 1H, $p\text{-cym iPr-H}$), 2.24 (s, 3H, $p\text{-cym CH}_3$), 1.26 (d, 3H, $J = 5.5$ Hz, $p\text{-cym iPr-CH}_3$), 1.17 (d, 3H, $J = 4.5$ Hz, $p\text{-cym iPr-CH}_3$; Figure S5). ^1H NMR ($\text{DMSO-}d_6$, 400 MHz, 298 K): δ (ppm) 7.88 (s, 1H, $\text{H}-\text{C}=\text{N}$), 7.09 (td, 1H, $J_1 = 8.0$ Hz, $J_2 = 2.0$ Hz, phenyl-H), 6.98 (dd, 1H, $J_1 = 7.6$ Hz, $J_2 = 1.6$ Hz, phenyl-H), 6.63 (d, 1H, $J = 8.4$ Hz, phenyl-H), 6.28 (t, 1H, $J = 8.0$ Hz, phenyl-H), 5.69 (d, 1H, $J = 5.6$ Hz, $p\text{-cym-H}$), 5.55 (d, 1H, $J = 6.4$ Hz, $p\text{-cym-H}$), 5.47 (d, 1H, $J = 6.0$ Hz, $p\text{-cym-H}$), 5.22 (d, 1H, $J = 6.0$ Hz, $p\text{-cym-H}$), 4.67 (m, 1H, $\text{N}-\text{CH}_2-$), 4.25 (m, 1H, $\text{N}-\text{CH}_2-$), 4.13 (m, 1H, $-\text{CH}_2\text{Cl}$), 4.04 (m, 1H, $-\text{CH}_2\text{Cl}$), 2.62 (m, 1H, $p\text{-cym iPr-H}$), 2.04 (s, 3H, $p\text{-cym CH}_3$), 1.11 (d, 3H, $J = 7.2$ Hz, $p\text{-cym iPr-CH}_3$), 1.02 (d, 3H, $J = 6.8$ Hz, $p\text{-cym iPr-CH}_3$; Figure S6). $^{13}\text{C}\{^1\text{H}\}$ NMR (CDCl_3 , 125 MHz, 298 K): δ (ppm) 165.5, 135.3, 134.7, 122.4, 118.8, 114.5, 101.9, 98.1, 86.1, 82.9, 81.5, 80.3, 70.6, 42.8, 30.5, 22.7, 21.6, 18.5 (Figure S7). UV-vis [MeOH , λ_{max} nm ($\epsilon/\text{M}^{-1}\text{cm}^{-1}$): 294 (5040), 388 (2020). IR (KBr pellets cm^{-1}): 1619 (s), 1449 (s), 1332(s), 762 (m). ESI-HRMS (MeOH): m/z (exp) 418.0509 (418.0506) $[\text{Ru}^{\text{II}}\text{C}_{19}\text{H}_{23}\text{ClNO}]^+$. Elemental analysis calcd (%) for $\text{C}_{19}\text{H}_{23}\text{Cl}_2\text{NORu}$: C 50.34, H 5.11, N 3.09. Found: C 50.18, H 5.19, N 2.98.

$[\text{Ru}^{\text{II}}(\text{L2})(\eta^6\text{-p-cym})\text{Cl}]$ (2). Yield: 68%. ^1H NMR (CDCl_3 , 500 MHz, 298 K): δ (ppm) 7.72 (s, 1H, $\text{H}-\text{C}=\text{N}$), 6.73 (dd, 1H, $J_1 = 7.5$ Hz, $J_2 = 1.5$ Hz, phenyl-H), 6.58 (dd, 1H, $J_1 = 8.0$ Hz, $J_2 = 1.5$ Hz, phenyl-H), 6.36 (t, 1H, $J = 7.6$ Hz, phenyl-H), 5.48 (m, 3H, $p\text{-cym-H}$), 5.10 (d, 1H, $J = 5$ Hz, $p\text{-cym-H}$), 4.51–3.84 (m, 4H, $\text{N}-\text{CH}_2-\text{CH}_2-\text{Cl}$), 3.80 (s, 3H, phenyl- OCH_3), 2.82 (m, 1H, $p\text{-cym iPr-H}$), 2.21 (s, 3H, $p\text{-cym CH}_3$), 1.23 (d, 3H, $J = 6.8$ Hz, $p\text{-cym iPr-CH}_3$), 1.15 (d, 3H, $J = 5.3$ Hz, $i\text{Pr-CH}_3$; Figure S9). $^{13}\text{C}\{^1\text{H}\}$ NMR (CDCl_3 , 125 MHz, 298 K): δ (ppm) 165.3, 157.0, 152.7, 126.1, 118.7, 115.0, 113.4, 102.1, 98.0, 85.7, 83.0, 81.6, 80.5, 70.6, 56.1, 42.9, 30.5, 22.7, 21.6, 18.5 (Figure S10). UV-vis [MeOH , λ_{max} nm ($\epsilon/\text{M}^{-1}\text{cm}^{-1}$): 298 (6620), 394 (2160). IR (KBr pellets cm^{-1}): 1618 (s), 1469 (s), 1218(s), 738 (m). ESI-HRMS (MeOH): m/z (exp) 448.0609 (448.0612) $[\text{Ru}^{\text{II}}\text{C}_{20}\text{H}_{25}\text{ClNO}]^+$. Elemental analysis calcd (%) for $\text{C}_{20}\text{H}_{25}\text{Cl}_2\text{NO}_2\text{Ru}$: C 49.65, H 5.21, N 2.90. Found: C 49.42, H 5.30, N 3.18.

General Procedure for the Preparation of Pt^{II} Complexes (3 and 4). To a methanolic solution, the respective ligands (0.1 mmol) and sodium acetate (0.1 mmol) were added followed by stirring for 15 min at 25 °C. Then, the 15 mL methanolic solution of $\text{Pt}(\text{DMSO})_2\text{Cl}_2$ (0.1 mmol) was added under nitrogen at 25 °C

and stirred for 24 h in the dark. The volume of the reaction mixture was reduced using a rotary evaporator at 35 °C, and few drops of diethyl ether were added to it. A yellow precipitate formed which was washed twice with diethyl ether and finally dried in a vacuum.

$[\text{Pt}^{\text{II}}(\text{L1})(\text{DMSO})\text{Cl}]$ (3). Yield: 70%. ^1H NMR (CDCl_3 , 400 MHz, 298 K): δ (ppm) 7.81 (s, 1H, $\text{H}-\text{C}=\text{N}$), 7.43 (m, 1H: phenyl-H), 7.26 (d, 1H, $J = 8$ Hz, phenyl-H), 7.13 (d, 1H, $J = 8.4$ Hz, phenyl-H), 6.70 (t, 1H, $J = 6.8$ Hz, phenyl-H), 4.55 (t, 2H, $J = 4.6$ Hz, $\text{N}-\text{CH}_2-$), 3.87 (t, 2H, $J = 5.3$ Hz, $-\text{CH}_2\text{Cl}$), 3.62 (s, 6H, DMSO-H ; Figure S12). $^{13}\text{C}\{^1\text{H}\}$ NMR ($\text{DMSO-}d_6$, 125 MHz, 298 K): δ (ppm) 164.5, 162.2, 135.9, 134.0, 118.9, 116.6, 63.4, 46.6, 40.4 (Figure S13). UV-vis [MeOH , λ_{max} nm ($\epsilon/\text{M}^{-1}\text{cm}^{-1}$): 290 (4240), 388 (1386). IR (KBr pellets cm^{-1}): 1604 (s), 1439 (s), 1133 (s), 743 (m). ESI-HRMS (MeOH): m/z (exp) 512.9723 (512.9741) $[\text{Pt}^{\text{II}}\text{C}_{11}\text{H}_{15}\text{Cl}_2\text{NO}_2\text{SNa}]^+$. Elemental analysis calcd (%) for $\text{C}_{11}\text{H}_{15}\text{Cl}_2\text{NO}_2\text{PtS}$: C 26.89, H 3.08, N 2.85. Found: C 26.75, H 3.14, N 2.74.

$[\text{Pt}^{\text{II}}(\text{L2})(\text{DMSO})\text{Cl}]$ (4). Yield: 72%. ^1H NMR ($\text{DMSO-}d_6$, 500 MHz, 298 K): δ (ppm) 8.19 (s, 1H, $\text{H}-\text{C}=\text{N}$), 7.06 (d, 1H, $J = 7.5$ Hz, phenyl-H), 7.02 (d, 1H, $J = 8$ Hz, phenyl-H), 6.60 (t, 1H, $J = 8$ Hz, phenyl-H), 4.52 (t, 2H, $J = 5.0$ Hz, $\text{N}-\text{CH}_2-$), 4.07 (t, 2H, $J = 5.0$ Hz, $-\text{CH}_2\text{Cl}$), 3.75 (s, 3H, phenyl- OCH_3), 2.54 (s, 6H, DMSO-H ; Figure S14). $^{13}\text{C}\{^1\text{H}\}$ NMR ($\text{DMSO-}d_6$, 125 MHz, 298 K): δ (ppm) 164.9, 154.1, 150.0, 125.9, 121.0, 118.1, 116.4, 63.7, 56.7, 47.1, 40.8 (Figure S15). UV-vis [MeOH , λ_{max} nm ($\epsilon/\text{M}^{-1}\text{cm}^{-1}$): 302 (8560), 402 (1840). IR (KBr pellets cm^{-1}): 1612 (s), 1470 (s), 1125 (s), 742 (m). ESI-HRMS (MeOH): m/z (exp) 542.9876 (542.9846) $[\text{Pt}^{\text{II}}\text{C}_{12}\text{H}_{17}\text{Cl}_2\text{NO}_3\text{SNa}]^+$. Elemental analysis calcd (%) for $\text{C}_{12}\text{H}_{17}\text{Cl}_2\text{NO}_3\text{PtS}$: C 27.65, H 3.29, N 2.69. Found: C 27.42, H 3.17, N 2.81.

X-ray Crystallography. Single crystals of complexes (2 and 4) were obtained using a slow evaporation method from methanol or dichloromethane solution, respectively. A suitable crystal for the respective complex was mounted on a loop of a goniometer of an Agilent SuperNova, Dual, Cu at zero, Eos diffractometer at 100 K. The data were collected using a monochromatic $\text{Mo K}\alpha$ ($\lambda = 0.71073$ Å) source and collected at 100 K. The data reduction was performed in CrysAlisPro 171.37.33c and solved either with the ShelXS structure solution program for complex 2 or ShelXT structure solution program for complex 4 using Olex2.⁴³ For complex 2, the data were solved with the ShelXS⁴⁴ structure solution program using direct methods. Complex 4 was solved with the ShelXT⁴⁵ structure solution program using Intrinsic Phasing. Both the structures were refined in ShelXL⁴⁶ refinement package using least squares minimization. All non-hydrogen atoms were refined with anisotropic displacement. The hydrogen atoms were fixed as per hybridization using ShelXL. Complex 4 showed multiple residual electron densities along with nonpositive definite (N.P.D.) on the heavy-atom center due to poor quality of the crystals. The single crystal data results showed no improvement upon change to other relevant space groups while solving or using the TWIN command during the refinement of the structure. The nonpositive definite (N.P.D.) on the heavy-atom center remained during the above changes. There are multiple spurious electron densities within 1.2 Å of the Pt(II) center represented in the CIF alerts. We are presenting the structure only for the benefit of the readers, but all the data presented for the Pt(II) structure should be accordingly interpreted keeping in mind the limitations of the X-ray diffraction data presented. The structures of complexes 2 and 4 were submitted in <https://www.ccdc.cam.ac.uk/deposit>. The CCDC numbers of complexes 2 and 4 are 1992724 and 1992723, respectively.

Kinetics and Binding Studies: ^1H NMR and ESI-MS Experiments. The samples for NMR experiments were prepared in 9:1 (v/v) phosphate buffer in D_2O (20 mM, pH 7.4, containing 4 mM NaCl) and $\text{DMSO-}d_6$ or CD_3CN , and the data were recorded on either a JEOL ECS 400 or a 500 MHz Bruker Advance III spectrophotometer. The ESI-MS samples were prepared in 9:1 (v/v) phosphate buffer (5 mM, pH 7.4, containing 4 mM NaCl) and MeOH , which was diluted in HPLC grade methanol.

CT DNA Binding Study. The stock solution of calf thymus (CT) DNA was prepared in 50 mM Tris-NaCl solution at pH 7.4 and kept for 10 h at 4 °C. The UV–visible spectrum showed that the A_{260} to A_{280} ratio was 1.9, indicating adequately pure, protein-free DNA. The concentration of the DNA was determined from the absorbance at 260 nm using the molar extinction coefficient ($6600 \text{ M}^{-1} \text{ cm}^{-1}$),⁴⁷ and the concentration was obtained by using an average of three independent measurements of the same stock solution. The target concentration ($1 \times 10^{-2} \text{ M}$) was prepared with proper dilution from a stock solution. The stock solution of the DNA was stored at 4 °C and used within 4 days. The DNA binding titration was carried out by the addition of 5 μL of CT DNA solution ($1 \times 10^{-2} \text{ M}$) in aliquots to solutions of $1.5 \times 10^{-4} \text{ M}$ complex **1** and $5 \times 10^{-4} \text{ M}$ complex **3** in 1% MeOH–50 mM Tris-HCl buffer (pH 7.4) in a 1 cm path length quartz cuvette of capacity 1.0 mL. The interaction of **1** and **3** with CT DNA was measured with the help of UV–vis spectroscopy. The change in absorbance at 291 and 287 nm for **1** and **3**, respectively, was monitored with the subsequent addition of aliquots of 5 μL of the DNA to the sample and reference cuvettes, allowing 5 min of equilibration before each reading. The titration was continued until there was no significant change in absorbance for at least three successive additions.

Cell Lines and Culture Conditions. Human pancreas ductal adenocarcinoma (MIA PaCa-2), triple negative human metastatic breast adenocarcinoma (MDA-MB-231), human hepatocellular carcinoma (Hep G2), and human colon adenocarcinoma (HT-29) were obtained from NCCS, Pune, India. The cells were grown in T-75 flasks as an adherent monolayer in a 5% carbon dioxide atmosphere using a culture medium, supplemented with 10% fetal bovine serum (GIBCO) and antibiotics (100 units mL^{-1} penicillin and 100 $\mu\text{g mL}^{-1}$ streptomycin). Hep G2 was grown in Minimal Essential Medium (MEM), while MIA PaCa-2 and HT-29 were cultured in Dulbecco's Modified Eagle Medium (DMEM). MDA-MB-231 was grown in a 1:1 mixture of DMEM with Ham's F12 nutrient mixture (*i.e.*, DMEM/F-12) and all cell lines were maintained at the logarithmic phase of growth before each experiment and plated when it reached 70% of confluence.

Cell Viability Assay. The growth inhibitory effect toward cancer cell lines (MIA PaCa-2, MDA-MB-231, Hep G2, and HT-29) was evaluated with the help of an MTT assay. In brief, 6×10^3 cells per well were seeded in 96-well microplates in respective media (200 μL) and incubated at 37 °C in a 5% carbon dioxide atmosphere. After 48 h of incubation, the medium was renewed (200 μL). Compounds to be studied were added at appropriate concentrations. Each concentration was tested in triplicate in the wells. The incubation was continued for 48 h. Upon completion of incubation with the compounds, the drug containing medium was removed, and 200 μL of fresh medium was added to each well followed by treatment with 20 μL of a 1 mg mL^{-1} MTT in 1 \times PBS (pH 7.2). After 3 h of incubation with MTT solution at 37 °C, the medium was removed, and the resulting formazan crystals were dissolved in DMSO (200 μL). The growth inhibitions of cells were analyzed by measuring the absorbance of the drug treated wells with respect to untreated ones at 595 nm using a BIOTEK ELx800 plate reader. IC_{50} values (drug concentrations responsible for 50% cell growth inhibition) were calculated by fitting nonlinear curves in GraphPad Prism 5 Ver 5.03, using a variable slope model constructed by plotting cell viability (%) vs the log of drug concentration in micromolarity.

Distribution Coefficient Determination. The distribution coefficient of the complexes (**1–4**) was determined in octanol and water containing 0.2 M NaCl (to suppress the tendency of hydrolysis) using a standard shake-flask method by shaking two layers for 6 h at 37 °C. Each set was performed in triplicate, and the absorbance was recorded with a UV–vis spectrophotometer using proper dilution. Distribution coefficient values ($\log D_{o/w}$) of complexes **1–4** were obtained from the ratio of the complex concentration present in octanol and water.

Metal Accumulation Study in MDA-MB-231 Cells by ICP-MS. In a 100 mm sterile tissue culture Petri-dish, 1.5×10^5 of MDA-MB-231 cells were seeded and grown for 48 h. Then, the cells were

treated with 20 μM (**1** and **2**) and 5 μM (**3** and **4**) of complex solutions for an additional 12 h. Subsequently, the medium was discarded, and the cells were washed using 1 \times -PBS (pH 7.2). The cells were then counted accurately after trypsinization for each drug treated sample. A total of 1×10^6 cells from each sample were counted and centrifuged to form a cell pellet. The cell pellets were washed twice by redispersing in 1 \times PBS (pH 7.2) followed by centrifugation. Cell pellets were then digested with 200 μL of extra pure (70% v/v) nitric acid (Sigma-Aldrich) at 70 °C for 12 h. The digested cell suspension was diluted using Milli-Q water, and the ruthenium and platinum content in the samples were analyzed on a Thermo Scientific iCAPRQ ICP-MS instrument at the SRIC facility IIT Kharagpur. Ruthenium and platinum standard solutions were freshly prepared to generate the calibration curve. All the samples were carried out in triplicate, and the standard deviations were calculated.

Detection of Apoptosis: Annexin-V Assay. Apoptotic cells were detected using a PE-Annexin V and 7-AAD dual staining apoptosis detection kit (BD Pharmingen) by flow cytometry according to the manufacturer's protocol. A total of 5×10^5 cells of MDA-MB-231 were seeded into a 100 mm sterile tissue culture Petri dish using 6 mL of DMEM+F-12 medium. Then, cells were incubated at 37 °C in a 5% carbon dioxide atmosphere for 48 h. Subsequently, the medium was changed and cells were treated with different concentrations of drug solutions of **1** and **3** for 24 and 12 h, respectively. Cells were then harvested using cold 1 \times PBS containing 0.1 mM EDTA and subsequently washed twice with cold 1 \times PBS and finally resuspended in Annexin V binding buffer. Cells were then incubated with both Annexin V-PE and 7-AAD for 15 min under dark conditions at 25 °C. Data were analyzed in a BD Biosciences FACS Calibur flow cytometer within 1 h of sample preparation.

Cell Cycle Analysis. MDA-MB-231 cells, 1×10^5 per plate, were seeded in a 90 mm Petri dish in a DMEM-F12 culture medium and incubated at 37 °C in a 5% carbon dioxide atmosphere. After 48 h, the medium was discarded and fresh medium added. Then, adequate concentrations of complexes **1** and **3** were added and incubated for 36 and 12 h, respectively. After drug exposure, cells were harvested by quick trypsinization and washed twice with cold 1 \times PBS (pH 7.2). Cells were resuspended in 100 μL of cold 1 \times PBS and were fixed with 70% aqueous ethanol overnight at 4 °C. DNA staining was performed by resuspending the cell pellets in 1 \times PBS solution comprised of PI ($55 \mu\text{g mL}^{-1}$) and RNase A ($100 \mu\text{g mL}^{-1}$) solution. The cell suspension was gently mixed with PI staining solution and incubated at 37 °C for half an hour. Samples were analyzed in BD Biosciences FACS Accuri and FACS Calibur flow cytometers.

Western Blot. MDA-MB-231 cells were cultured on 100 mm dishes to 70% confluency and treated with 1 μM of **3** for 8 h. Cell pellets were washed with phosphate buffered saline (pH = 7.2) and suspended in 90 μL of RIPA lysis buffer. The resuspension was incubated on ice for 1 h with occasional mixing. The cell suspension was lysed using an ultrasonic probe sonicator. The resultant homogenate was centrifuged at 800g for 10 min followed by collection of the supernatant. The total protein in the lysate was estimated by Bradford (Sigma-Aldrich) assay. A total of 120 μg (control and treated) of lysate was mixed with gel loading dye (2% SDS, 2.5% β mercapto-ethanol, 7.5% glycerol, 2 M urea, and 0.005% bromophenol blue). The mixture was adsorbed in 10% denaturing polyacrylamide gel and transferred to a nitrocellulose membrane (BioRad Laboratories) using chilled Towbin transfer buffer in a Trans-Blot SD semidry transfer cell at 15 mA current for 50 min. The membrane was blocked with 5% skim milk (Sisco Research Laboratories) in TBST (Tris buffered saline with 0.1% Tween-20) at room temperature for 2 h and incubated overnight at 4 °C with primary antibody [cyclin D (abcam) and Bcl-2 (abcam) 1:1000] in 3% skim milk and 0.1% tween-20. Membrane is washed thrice with TBST. The resultant membrane was then incubated in goat anti-rabbit HRP (BioBharati India) conjugated secondary antibody (abcam) for 2 h at room temperature followed by washing in TBS-T (thrice) and in TBS (twice). The chemiluminescence (clarity max,

Biorad) was detected using a ChemiDoc Imaging System (170–01401) (Bio-Rad) instrument.

Optical Microscopy Imaging. MDA-MB-231 cells were seeded at 1.2×10^4 per well in a six-well plate and were grown on a coverslip with 2 mL of DMEM-F12. After 48 h, the existing medium was replaced with a fresh one and incubated with the required concentrations of **1** and **3** for 12 h. After removal of drug containing media, cells were fixed with a 4% para formaldehyde solution in 1× PBS (pH 7.2). Then the cells were incubated with DAPI ($1 \mu\text{g mL}^{-1}$) followed by washing several times. The optical microscopy images of MDA-MB-231 cells were acquired using a Leica SP8 confocal microscope. Both DIC and fluorescence microscopy were processed using *LASX* and *ImageJ* software.

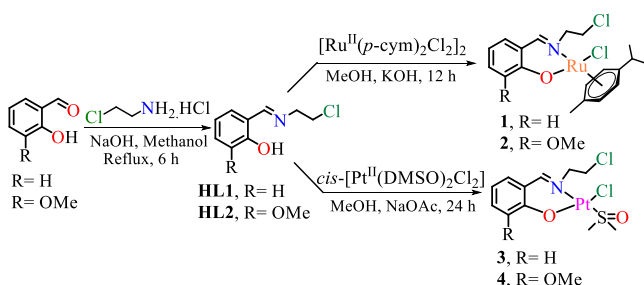
Mitochondrial Membrane Potential Determination by JC-1. Investigation of the change in mitochondrial transmembrane potential (MMP, $\Delta\Psi\text{m}$) was determined using flow cytometry after staining live cells with JC-1. A total of 5×10^5 MDA-MB-231 cells were seeded in a 100 mm Petri dish. After 48 h of incubation, medium was removed, and the cells were treated with complex **1** and **3** using IC_{25} and IC_{50} concentrations for 24 and 12 h, respectively. Cells were then harvested by removing the media and washed with 1× PBS. The entire washing was collected and centrifuged at 2000 rpm for 4 min. The cells were washed twice with 1× PBS and resuspended in 1× PBS supplemented with 10% FBS. The resultant solution was then incubated with $5 \mu\text{g/mL}$ JC-1 dye for 30 min in the dark. Finally, after removing the supernatant, the cells were suspended in 1× PBS and analyzed in a BD Bioscience FACS Calibur flow cytometer by measuring the red and green fluorescent intensities.

Caspase 3 Activation Assay. Activation of Caspase 3 due to complex treatment was investigated against MDA-MB-231 using a Caspase 3 colorimetric detection kit (Sigma). The manufacturer's protocol was followed throughout the assay. In brief, 5×10^5 MDA-MB-231 cells were first seeded in a 100 mm sterile tissue culture Petri dish for 48 h. Cells were then treated with both IC_{25} and IC_{50} concentrations of complexes **1** and **3** for 24 and 12 h, respectively. Release of p-nitroaniline was monitored with time after caspase 3 substrate treatment with the cell lysate. The assay was performed following the 96 well plate method, and data were recorded using an ELISA plate reader at 405 nm. The standard curve was drawn using a known concentration of pNA (p-nitroaniline) to estimate the amount of pNA released by Caspase 3.

RESULTS AND DISCUSSION

Synthesis and Characterization. The ligands **HL1** and **HL2** were synthesized by condensation of 2-chloroethylamine hydrochloride with salicylaldehyde or o-vanillin, respectively, following a modified literature procedure.^{42,48} The ligands were characterized with ^1H and $^{13}\text{C}\{^1\text{H}\}$ NMR. The Ru-*p*-cymene complexes (**1** and **2**) were synthesized by the reaction of the respective deprotonated ligands with $[\text{Ru}^{\text{II}}(\eta^6\text{-p-cym})_2(\text{Cl})_4]$ in degassed methanol at room temperature for 12 h (Scheme 1). Stirring **HL1** and **HL2** in methanol followed by the addition of sodium acetate (NaOAc) and *cis*-

Scheme 1. Synthetic Procedure for the Preparation of Ligands (HL1 and HL2) and Metal Complexes (1–4)



$[\text{Pt}(\text{DMSO})_2\text{Cl}_2]$ under an inert atmosphere at room temperature for 24 h gave complexes **3** and **4** (Scheme 1). All the complexes are new and air-stable solids isolated in moderate to high yields. Characterization by NMR, ESI-HRMS, UV–vis, IR, single-crystal X-ray diffraction, and elemental analysis showed the purity and structural aspects of the complexes.

The four aromatic protons in the *p*-cymene ring of the Ru(II) complexes **1** and **2** show a splitting pattern of 3 + 1 in the ^1H NMR using CDCl_3 . This suggests that the δ values of those three protons are very close to each other in CDCl_3 and therefore appear as a multiplet in the δ 5.4–5.1 ppm region (Figures S5 and S9). In order to further confirm the result, we performed the ^1H NMR of complex **1** in $\text{DMSO-}d_6$ and found that the splitting pattern changed to (1 + 1 + 1 + 1) for the four-aromatic *p*-cymene protons in δ 5.7–5.2 ppm (Figure S6). In the case of **1**, the two quaternary carbons of the aromatic ring of the **L1** possess the same chemical shift, as suggested by the HMQC spectra (Figure S8). Furthermore, in the case of **2**, one of the $-\text{CH}_2$ protons of the chloroethylamine group and the $-\text{OCH}_3$ protons of the aromatic ring of **L2** possess the same chemical shift, which is also confirmed from the HMQC spectra (Figure S11), since the chemical shift of their corresponding carbons are different. The stretching frequency corresponding to the $\text{C}=\text{N}$ of the imine and the $\text{C}-\text{Cl}$ bond of chloroethylamine appears in the range of 1600–1620 and 730–760 cm^{-1} , respectively, in all complexes. In the cases of **1** and **2**, the UV–vis spectroscopy in methanol showed an intense band at around 228–240 nm that may be attributed to $\pi-\pi^*$ transitions. The relatively weak bands at around 290–300 nm and 380–400 nm may be assigned to $n-\pi^*$ and MLCT transitions, respectively.^{49,50} In the cases of **3** and **4**, similar transitions appear at 225–230, 288–305, and 390–405 nm, respectively. The complexes are neutral, so in the ESI-MS positive ionization mode, the *m/z* corresponds to the following formulations, $[\text{Ru}(\text{L1/L2})(\text{p-cym})]^+$ for the Ru(II) and $[\text{Pt}(\text{L1/L2})(\text{DMSO})(\text{Cl})\text{Na}]^+$ for the Pt(II) complexes.

X-ray Crystallography. The crystals of complexes **2** and **4** were obtained using a slow evaporation method from methanol and dichloromethane solution at 25 °C. The crystal structures show the pseudo-octahedral and distorted square planar geometries of the metal centers in **2** and **4**, respectively (Figure 2A and B). Complex **2** crystallizes in the orthorhombic system with space group $P2_1/n$, whereas **4** crystallizes in the monoclinic system with space group $Pna2_1$ (Table 1). Each unit cell of complexes **2** and **4** contains four and eight molecules, respectively (Figure S17). There are no intra- or intermolecular hydrogen bonding interactions observed in the unit cell of either **2** or **4**. The metal center is in a +2 oxidation state in both the complexes. The +2 charge on the metal ion is neutralized by a phenolic oxygen of ligand **HL2** and a monodentate chlorido ligand (Figure 2A and B). Two of the metal coordination sites are occupied by the N,O donor **L2**. The length of the Ru–O bond is similar to Ru–N bond with distances of 2.0822(15) Å and 2.0881(18) Å, respectively. The crystal of the Pt complex **4** was of relatively poor quality. The Pt–O and Pt–N bond lengths are ca. 2.01 and 2.03 Å, respectively (Table 2). The $\angle\text{O}-\text{Ru}-\text{N}$ and $\angle\text{O}-\text{Pt}-\text{N}$ angles are 88.05(6)° and ca. 91°, respectively (Table 2). In **2**, the other two coordination sites are occupied by an η^6 -bonded *p*-cymene and a monodentate chlorido ligand (Figure 2A). In contrast, the Pt(II) in **4**, apart from the N,O donor chelation by **L2**, coordinates to a S from dimethyl sulfoxide and a monodentate chlorido to complete the square planar

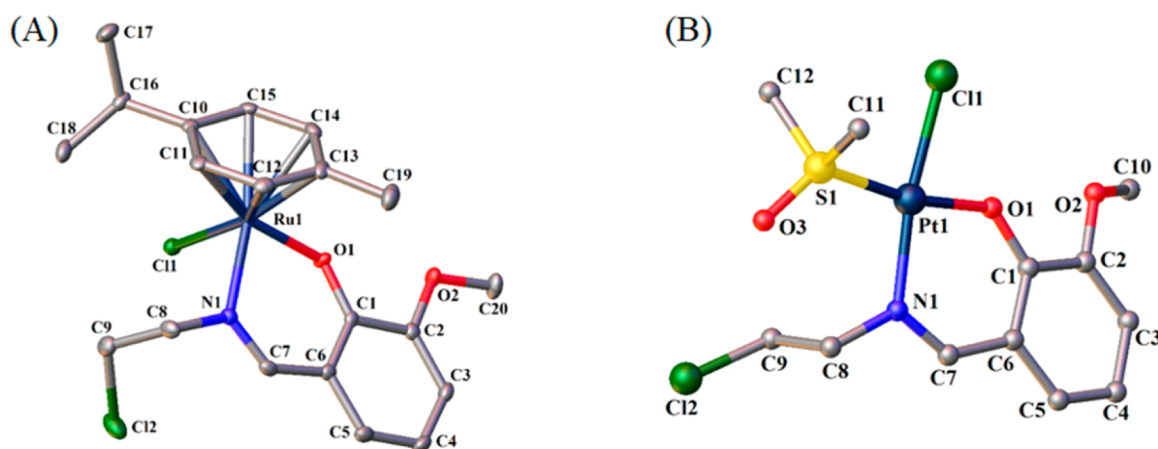


Figure 2. (A) ORTEP diagram of the molecular structure of complex **2** with 50% probability level, derived from X-ray single crystal structure. Hydrogen atoms are omitted for clarity. (B) Ball and stick diagram of the molecular structure of complex **4** was obtained from X-ray single crystal structure. Hydrogen atoms are omitted for clarity.

Table 1. Selected Crystallographic Parameters of Complexes **2** and **4**

	2	4
empirical formula	C ₂₀ H ₂₉ Cl ₂ NO ₄ Ru	C ₁₂ H ₁₇ Cl ₂ NO ₃ PtS
formula weight	483.38	521.32
temperature (K)	100.01(10)	100.00(10)
radiation	Mo K α (λ = 0.71073 Å)	Mo K α (λ = 0.71073 Å)
crystal system	monoclinic	orthorhombic
space group	P2 ₁ /n	Pna2 ₁
<i>a</i> (Å)	9.8609(2)	12.8508(2)
<i>b</i> (Å)	11.7792(2)	7.09440(10)
<i>c</i> (Å)	18.3582(4)	34.2318(7)
α (deg)	90.00	90.00
β (deg)	90.2682(19)	90.00
γ (deg)	90.00	90.00
volume (Å ³)	2132.34(8)	3120.87(9)
<i>Z</i> , ρ_{calcd} (g/cm ³)	4, 0.506	8, 2.219
goodness-of-fit on <i>F</i> ²	1.124	1.095
independent reflections	4310 [Rint = 0.0276, Rsigma = 0.0241]	5394 [Rint = 0.0796, Rsigma = 0.0311]
final <i>R</i> indexes [all data]	<i>R</i> ₁ = 0.0247, ^a <i>wR</i> ₂ = 0.0576 ^b	<i>R</i> ₁ = 0.0408, ^a <i>wR</i> ₂ = 0.0984 ^b

$$^a R_1 = \sum |F_o| - |F_c| / \sum |F_o|, \quad ^b wR_2 = [\sum (w(F_o^2 - F_c^2)^2) / \sum w(F_o^2)^2]^{1/2}.$$

coordination (Figure 2B). In the case of **2**, all the Ru–C bonds are not equal. The Ru–C10 bond length (2.214(2) Å) is higher than that of Ru–C13 (2.173(2) Å) due to the presence of a sterically hindered isopropyl group at C10 (Table 2). In complex **4**, the \angle N–Pt–S, \angle N–Pt–O, \angle S–Pt–Cl, and \angle O–Pt–Cl are varying from ca. 83 to 100°, suggesting distorted square planar geometry at the Pt(II) center. The deviation from a perfect square planar structure may be due to higher steric bulk of DMSO repelling C8 and C9 from L2 (Table 2).

Hydrolysis Study. Complexes **1** and **3** hydrolyzed upon dissolution in 9:1 (v/v) phosphate buffer in D₂O (20 mM, pD 7.4, containing 4 mM NaCl) and DMSO-*d*₆ (for **1**) or acetonitrile-*d*₃ (for **3**), respectively. The ¹H NMR data of **1** show immediate hydrolysis within 5 min, and the hydrolyzed adduct is stable up to the monitored period of 24 h (Figure 3). This was concluded by ¹H NMR with the addition of AgNO₃, which provided the same ¹H NMR spectrum, implying

immediate hydrolysis in the buffer. Similar observations are well-known for N,O coordinated Ru–arene complexes.^{33,51}

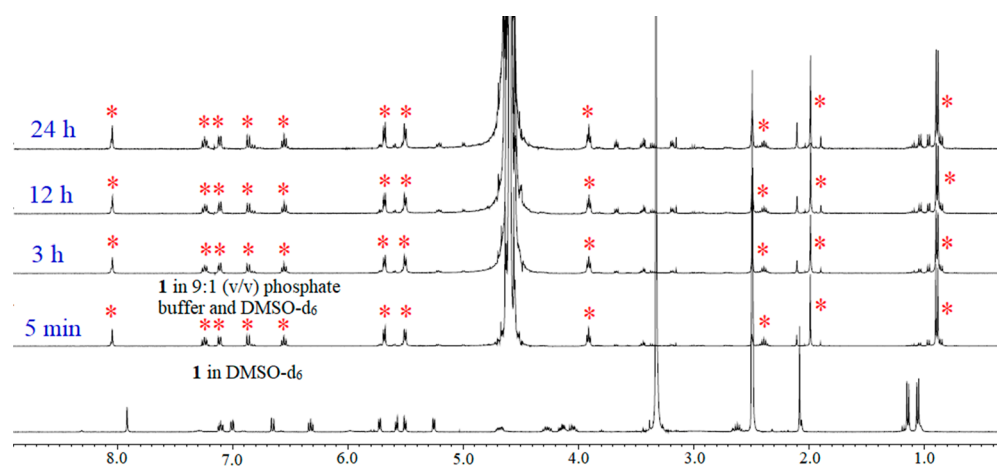
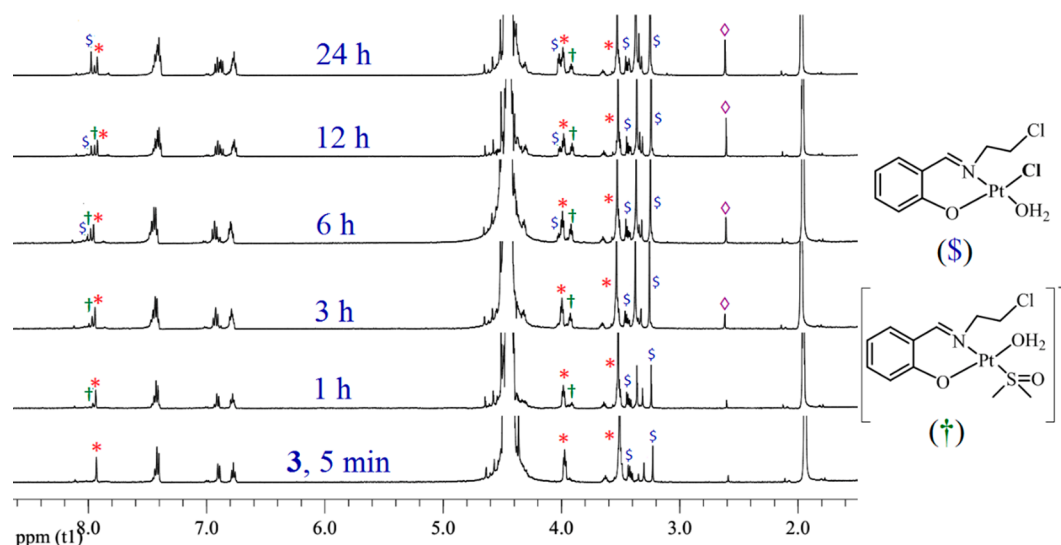
The ³¹P NMR also did not show any phosphate adduct of **1** even after 20 h. The presence of the hydrolyzed complex is also supported by positive mode ESI-MS, where we have found the cations of formulation [Ru(L1)(*p*-cym)]⁺ and [Ru(L1)(*p*-cym)Cl]Na⁺, which remain stable for up to a 24 h observed period (Figures S18 and S19). The ¹H NMR data of complex **3**, which has the same ligand with Pt(II) as the metal center, showed the formation of hydrolyzed adducts within 1 h (Figure 4), and even after 24 h, ca. 40% of the intact parent complex was present in the solution. However, the hydrolyzed adducts are stable up to 24 h, which is also confirmed by ESI-MS. The ESI-MS data in 9:1 (v/v) phosphate buffer (5 mM, pH 7.4, containing 4 mM NaCl) and methanol provides *m/z* values that match well with the formulations [Pt(L1)(DMSO)-OH]Na⁺, Pt(L1)(DMSO)(OH₂)⁺, and Pt(L1)Cl(OH₂)Na⁺ (Figures S20 and S21), which we have also assigned in the NMR spectra as probable speciations. The chemical environments of complexes **2** and **4** are similar to those of **1** and **3**, respectively. So, we monitored the hydrolysis of **2** and **4** only with ESI-MS (Figures S22–S26). The hydrolysis of **4** starts within 10 min (Figure S24) and is faster than that of **3**. However, similar to **1**, complex **2** shows immediate aquation and is stable upon aquation at least for the observed 24 h period (Figures S22 and S23).

The stabilities of the free ligands HL1 and HL2 were also monitored in 9:1 (v/v) phosphate buffer in D₂O (20 mM, pD 7.4, containing 4 mM NaCl) and DMSO-*d*₆. They were unstable in aqueous solution, and in 24 h ca. 60–80% of the ligands were dissociated into their corresponding amine and aldehyde (Figures S27 and S28). This may be one of the reasons that the ligands are nontoxic *in vitro*.

DNA Binding Studies. All four complexes were studied for their binding ability with model nucleobase 9-ethylguanine (9-EtG) either by ¹H NMR or by ESI-MS. The N⁷ position of guanine binds with the desired electrophilic site rendering a downfield chemical shift of the hydrogen next to N⁷. The ¹H NMR spectra of **1** with 2 mol equiv of 9-EtG in 9:1 (v/v) phosphate buffer in D₂O (20 mM, pD 7.4, containing 4 mM NaCl) and DMSO-*d*₆ showed that the H8 proton of the 9-EtG is shifted from 7.64 to 8.06 ppm within 5 min of addition (Figure 5A). This shift is due to the formation of a

Table 2. Selected Bond Lengths (Å) and Bond Angles (deg) for Complexes 2 and 4

2				4			
Ru1 O1	2.0822(15)	O1 Ru1 N1	88.05(6)	Pt1 O1	2.007(11)	O1 Pt1 N1	90.9(5)
Ru1 N1	2.0881(18)	O1 Ru1 C10	143.93(7)	Pt1 N1	2.028(13)	O1 Pt1 Cl1	83.0(3)
Ru1 C10	2.214(2)	O1 Ru1 C11	161.04(7)	Pt1 Cl1	2.308(3)	O1 Pt1 S1	169.2(3)
Ru1 C11	2.202(2)	O1 Ru1 C12	124.62(7)	Pt1 S1	2.217(4)	N1 Pt1 S1	99.6(4)
Ru1 C12	2.161(2)	O1 Ru1 C13	92.42(7)			N1 Pt1 Cl1	172.0(4)
Ru1 C13	2.173(2)	O1 Ru1 C14	85.46(7)			S1 Pt1 Cl1	86.77(14)
Ru1 C14	2.178(2)	O1 Ru1 C15	107.10(7)				
Ru1 C15	2.202(2)	O1 Ru1 Cl1	84.20(4)				
Ru1 Cl1	2.4495(5)	N1 Ru1 C10	127.55(8)				
		N1 Ru1 C11	97.76(8)				
		N1 Ru1 C12	89.23(8)				
		N1 Ru1 C13	109.29(8)				
		N1 Ru1 C14	146.46(8)				
		N1 Ru1 C15	164.65(8)				
		N1 Ru1 Cl1	86.81(5)				

Figure 3. Stability of 1 in 9:1 (v/v) phosphate buffer in D₂O (20 mM pD 7.4, containing 4 mM NaCl) and DMSO-*d*₆. (*) Aquated complex of 1.Figure 4. ¹H NMR spectra of stability of 3 in 9:1 (v/v) phosphate buffer in D₂O (20 mM, pD 7.4, containing 4 mM NaCl) and acetonitrile-*d*₃. (*) Intact complex 3, (\$) DMSO released aquated complex of 3, (†) chlorido released aquated complex of 3, (◇) chemical shift of released DMSO. Formulations are assigned from ESI-MS.

monoadduct of 9-EtG, which is also supported by the ESI-MS, *m/z* at 597.1298 (calcd 597.1313) corresponding to the formulation [(1-Cl⁻) + 9-EtG]⁺ (Figures S5B, S29, and S30).

After 24 h, there was no further increase in the intensity of the peak observed. In the case of 2, the corresponding 9-EtG adduct appears at *m/z* 627.1467 (calcd 627.1419; Figures S31

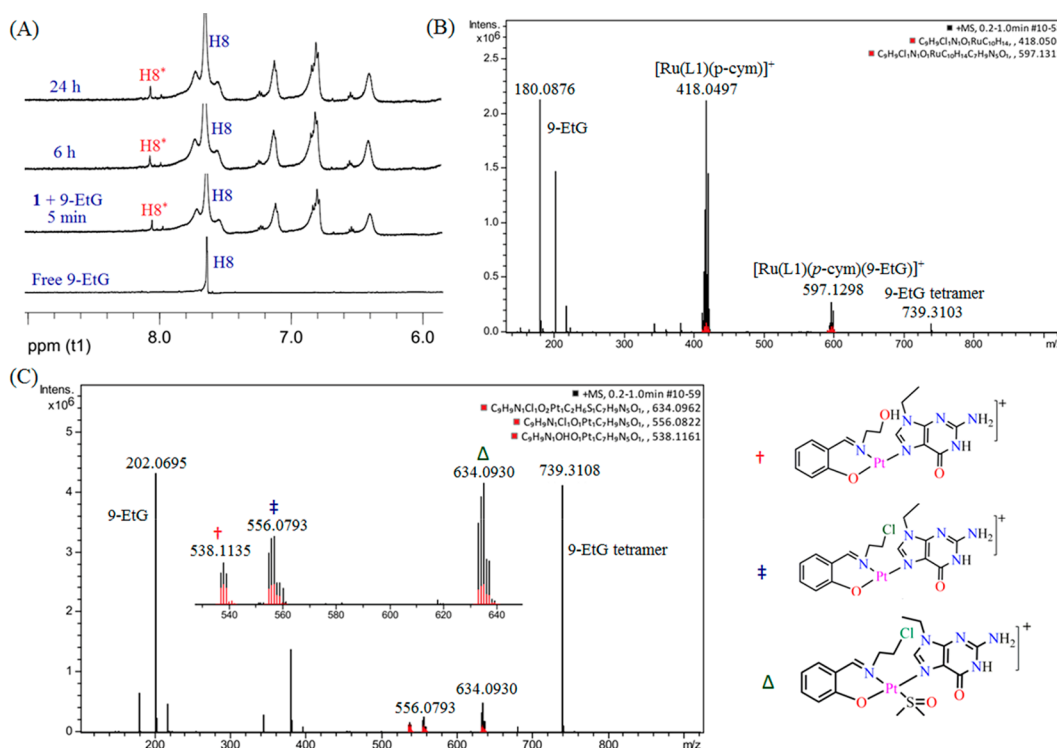


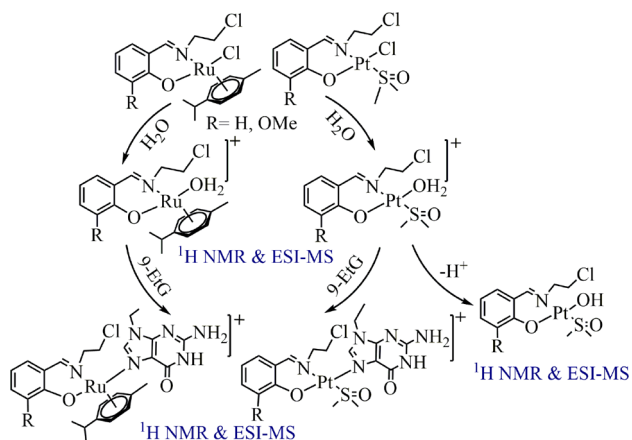
Figure 5. (A) ^1H NMR spectra of 9-ethylguanine (9-EtG) binding of **1** in 9:1 (v/v) phosphate buffer in D_2O (20 mM, pD 7.4, containing 4 mM NaCl) and $\text{DMSO-}d_6$. H8^* indicates shift of the H8 proton due to binding with 9-EtG. (B) ESI-MS spectra of 9-EtG binding of **1** in 9:1 (v/v) phosphate buffer (5 mM, pH 7.4, containing 4 mM NaCl) and methanol. (C) ESI-MS spectra of 9-EtG binding of **3** in 9:1 (v/v) phosphate buffer (5 mM, pH 7.4, containing 4 mM NaCl) and methanol. The chemical structures of different 9-EtG adducts of **3** are shown separately.

and **S32**) corresponding to the formulation $[(2\text{-Cl}^-) + 9\text{-EtG}]^+$. The Pt(II) complexes **3** and **4** also showed the formation of a mono-adduct of 9-EtG immediately within 10 min along with aquated **3** and **4**. After 24 h, only the 9-EtG bound complexes are present in the solution corresponding to m/z 634.0930 (calcd 634.0962) having formulation $[(3\text{-Cl}^-) + 9\text{-EtG}]^+$ and an m/z of 664.1020 (calcd 664.1067; Figures S3, S33, and S34) having formulation $[(4\text{-Cl}^-) + 9\text{-EtG}]^+$ (Figures S35 and S36). Hence, all the complexes display their potential as DNA binding agents (Scheme 2).

The interaction with 9-EtG warranted calf thymus (CT) DNA binding studies with **1** and **3** to represent their DNA

binding capability. The absorption spectral titration study with increasing concentration of DNA showed that the absorbance of **1** decreases (hypochromism) along with a bathochromic shift (~ 4 nm) with the increase in DNA concentration (Figure S37A). In contrast, the absorbance of complex **3** decreases (hypochromism) with a hypsochromic shift (~ 5 nm) with the increase in CT DNA concentration (Figure S37B). The above results imply structural changes to DNA and are usually a characteristic of metal complexes cross-linking CT DNA. The intrinsic binding constant (K_b) was calculated by plotting $[\text{DNA}]/(\epsilon_a - \epsilon_f)$ versus $[\text{DNA}]$. Complexes **1** and **3** have K_b values of $(3.7 \pm 1.2) \times 10^3 \text{ M}^{-1}$ and $(4.3 \pm 1.9) \times 10^3 \text{ M}^{-1}$, respectively (Figures S37 and S38). The binding constants (K_b) of the complexes suggest that the complexes are able to interact with DNA.

Scheme 2. Proposed Reaction Pathways of Ru and Pt Complexes (1–4) for Hydrolysis and Binding with 9-EtG based on ^1H NMR and ESI-MS Studies



Cytotoxicity Studies. The *in vitro* cytotoxicity of ligands **HL1** and **HL2** and their Ru(II) and Pt(II) complexes **1–4** was assessed toward four aggressive human cancer cell lines, Mia PaCa-2, MDA-MB-231, HepG2, and HT-29 cell lines. The cells were treated with different concentrations of complexes using the clinical drug cisplatin (CDDP) as a positive control with an exposure time of 48 h. The free ligands alone presented no cytotoxic effect up to $100 \mu\text{M}$. However, complexes **1–4** showed moderate to good cytotoxicity in the tested cell lines (Table 3, Figures S39–S42). The Ru(II) complexes **1** and **2** showed almost similar cytotoxicity in MIA PaCa-2, MDA-MB-231, and Hep G2, but **1** is more potent than **2** against HT-29. On the other hand, in the case of Pt(II) complexes, **3** and **4** display similar toxicity in all the tested cancer cell lines. However, the Pt(II) complexes **3** and **4** are *ca.* 10–20 times more cytotoxic than the Ru(II) complexes **1** and **2** (Table 3) against all the cancer cell lines investigated.

Table 3. Cytotoxicity of the Ligands and Metal Complexes in Various Cancer Cell Lines

complex	IC ₅₀ ± SD (μM) ^{a,b}			
	MIA PaCa-2	MDA-MB-231	Hep G2	HT-29
HL1	>100	>100	>100	>100
HL2	>100	>100	>100	>100
1	10.0 ± 1.1	21.1 ± 1.6	26.9 ± 1.0	49.3 ± 2.5
2	15.0 ± 0.5	31.1 ± 0.8	25.5 ± 1.1	>75
3	0.86 ± 0.1	1.23 ± 0.1	1.48 ± 0.1	2.63 ± 0.3
4	1.36 ± 0.1	1.34 ± 0.2	1.13 ± 0.1	3.83 ± 0.3
CDDP ^c	31.8 ± 4.8	37.2 ± 2.5	14.3 ± 0.8	>50

^aIC₅₀ ± SD (IC₅₀ = half-maximal inhibitory concentration; SD = standard deviation) are determined by MTT assay in normoxia (~15% O₂) for 48 h drug exposure, and values given are mean of at least three independent experiments. In a single experiment each concentration was assayed in triplicate. ^bThe statistical significance (*P*) of the IC₅₀ data ranges between >0.001 and <0.05. ^cCDDP: Cisplatin, data from our previous report done under similar experimental conditions.³³

Notably, all the complexes display the highest toxicity against MIA PaCa-2 and are more potent than CDDP, against the same. The higher cytotoxicity toward MIA PaCa-2 is also seen for several other nitrogen mustard coordinated Pt(II) complexes reported by us earlier.^{7,9,10}

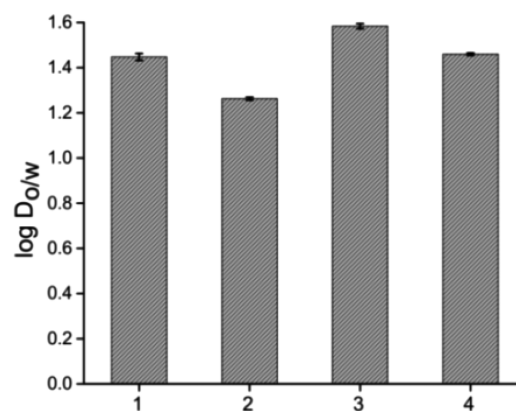
Thus, the presence of the chloroethylamine group in the complexes may be beneficial for their toxicity toward the pancreatic adenocarcinoma (MIA PaCa-2) whether the metal is Pt(II) or Ru(II). Encouragingly the Pt(II) complexes are also very efficient against the aggressive triple negative breast cancer (TNBC) MDA-MB-231 where chemotherapy is mostly the sole option, displaying an IC₅₀ (half-maximal inhibitory concentration) of *ca.* 1.5 μM. Complex 3 is the most efficient in the series and displayed 10–30 times more toxicity than CDDP against all the cancer cell lines tested. Hence, the above study suggests that the Pt(II) analogues are much more efficient than the Ru(II) analogues of the same ligands or the clinical drug CDDP.

The DMSO bound Pt(II) complexes are distorted square planar, and in aqueous solution the bound DMSO or the chlorido ligand is lost slowly over time. The Ru(II)-*p*-cymene analogues are pseudo-octahedral and the chlorido is lost almost instantaneously to form the aquated species. The aquated Ru complexes coordinated with a *p*-cymene (a π -donor ligand) may be rendering more electron density toward the Ru(II) center^{52,53} compared to that of the Pt(II) center having no such π -donor ligand, leading to higher reactivity of the Pt(II) complexes toward external nucleophiles (*viz.*, 9-EtG) and

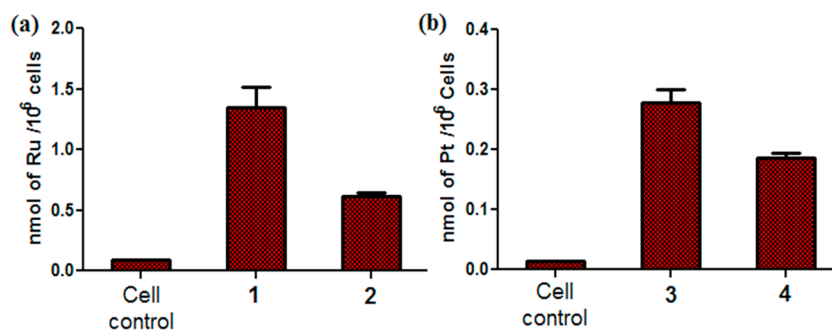
making them (3 and 4) more toxic than the Ru(II) complexes 1 and 2.

Cellular Internalization of the Complexes. The Ru and Pt contents (nmol of metal per 10⁶ cells), quantified by ICP-MS (Inductively coupled plasma mass spectrometry), in MDA-MB-231 cells showed a good correlation of cytotoxicity vs cellular internalization (Figure 6). The cells were treated with 20 μM Ru and 5 μM Pt complexes for 12 h. It has been observed that in the case of Ru complexes, the salicylaldehyde derivative (1) accumulates more than the corresponding o-vanillin analogue (2). The same trend was also observed for the Pt derivatives; however the difference in accumulation is not significant. This may be due to the lower dose of Pt complexes used for the accumulation study as a result of their high toxicity, which keeps us from making a comparison of cellular uptake between 3 and 4. However, the IC₅₀ values of the complexes (1–4; Table 3) especially in MDA-MB-231 agree well with the cellular accumulation data, showing a higher difference in cytotoxicity between 1 and 2 compared to 3 and 4.

Lipophilicity. The lipophilicity of biologically active compounds has a major impact on their capacity to cross through a cellular membrane, an important parameter to influence cytotoxicity. We measured the lipophilicity of the complexes (1–4) to see if there is any correlation between the lipophilicity and cellular internalization. The distribution coefficient (log *D*) values in the octanol/water system for 1–4 are in the range of 1.2–1.6 (Figure 7), suggesting the

**Figure 7.** Lipophilicity study of complexes 1–4 in the octanol–water mixture.

lipophilicity values are within the range of new pharmacophores as shown by the Comprehensive Medicinal Chemistry

**Figure 6.** Cellular accumulation study of (a) 1 and 2 (20 μM) and (b) 3 and 4 (5 μM) in MDA-MB-231 cells

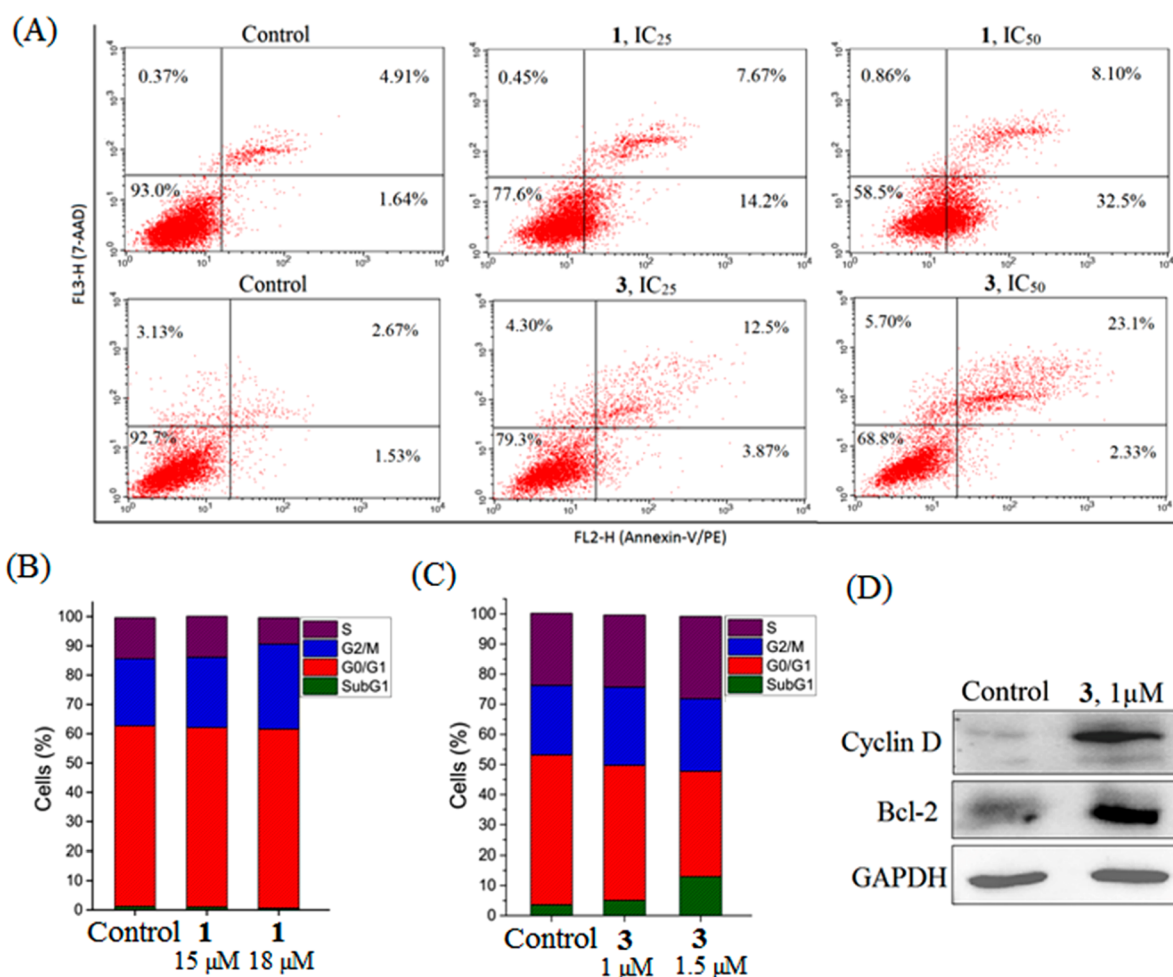


Figure 8. (A) Investigation of apoptosis by flow cytometry analysis of MDA-MB-231 cells after exposure to **1** for 24 h and **3** for 12 h after Annexin V-PE/7-AAD dual staining. Lower left quadrant (LL): intact cells. Lower right quadrant (LR): early apoptotic cells. Upper right quadrant (UR): late apoptotic cells. Upper left quadrant (UL): dead cells. (B) Cell cycle distribution of **1** in the MDA-MB-231 cell line after treatment with two sub-IC₅₀ concentrations of **1** for 36 h. (C) Cell cycle distribution of **3** in MDA-MB-231 cell line after treatment with different concentrations of **3** for 12 h. (D) Effects of **3** on Bcl-2 and cyclin D expression in MDA-MB-231 cells (Western blot). Glyceraldehyde 3-phosphate dehydrogenase (GAPDH) was used as the loading standard. All normalizations were performed with respect to GAPDH.

database.⁵⁴ All the complexes are similar in terms of lipophilicity, although **3** may be argued to be marginally higher. In spite of the small differences in lipophilicity, the cellular accumulation of **1** is almost double than that of **2** in MDA-MB-231, leading to a higher efficacy of **1** against the same. However, for **3** and **4**, the cytotoxicity values are similar in most of the cell lines, which agrees well with the lipophilicity data.

Mechanism of Cell Killing. Complexes **1** and **3** were further investigated for mechanistic differences, if any, between the Pt(II) and Ru(II) complexes. The flow cytometry results show that both the Ru(II) and Pt(II) complexes kill the cells via apoptosis. **1** and **3** induce apoptosis at IC₅₀ and sub-IC₅₀ doses. Treatment with **1** for 24 h induced 22–40% apoptosis at IC₂₅ and IC₅₀ doses. Similarly, **3** induced 16–25% apoptosis at IC₂₅ and IC₅₀ doses after treatment for 12 h (Figure 8A). The shrinkage of cells with condensed (early apoptosis) or fragmented (late apoptosis) nuclei compared to the control cells (Figure S43) upon treatment with **1** and **3** also supports apoptosis to be the pathway of cellular death. A careful observation of the Annexin V-PE/7-AAD plot (Figure 8A) shows that there are more cells with late apoptosis in the Pt(II)

complex **3** in spite of short incubation time and lower dose used. The distorted square planar geometry of the Pt(II) may be making the complexes more reactive compared to the pseudo-octahedral Ru(II) complex **1** as discussed earlier.

The cell cycle was analyzed by measurement of the DNA content of **1** and **3** treated MDA-MB-231 cells; using flow cytometry by treatment with two different concentrations of **1** and **3** showed cell cycle arrest in mostly the G2/M phase for **1** (Figures 8B and S44) and SubG1 phase for **3** (Figures 8C and S45). Complex **3** also arrests the cell cycle in the S phase, which suggests indirectly that DNA may be one of the possible targets. The cell cycle arrest data of complexes **1** and **3** suggest that they act through different pathways to kill the cells. In addition, compared to our earlier work with the nitrogen mustard based Pt(II) complexes which arrest the cell cycle mostly in G2/M phase, the chloroethylamine bearing Pt(II) complex **3** shows a different pathway of cell killing through SubG1 phase arrest.

The change in the pathway of cell cycle arrest by **3**, compared to our earlier Pt(II/IV) mustard ligand-based complexes, may be assigned to the change of the ligand part to chloroethylamine instead of the bis(2-chloroethyl)-

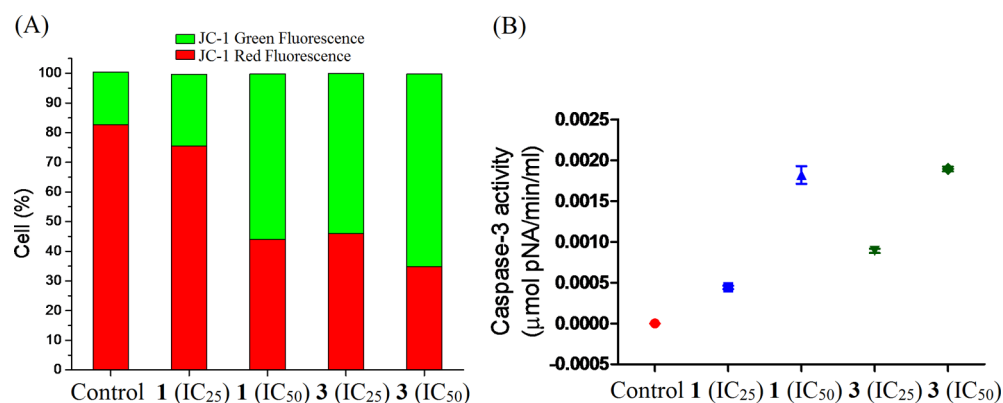


Figure 9. (A) Dose-dependent increase in depolarization of mitochondria in MDA-MB-231 cells after treatment with IC₂₅ and IC₅₀ concentrations of **1** and **3** for 24 and 12 h, respectively. (B) Colorimetric determination showing caspase-3 activation in the MDA-MB-231 cell line with **1** and **3** with IC₂₅ and IC₅₀ concentrations for 24 and 12 h, respectively.

amine.^{7,9,10} The attached DMSO is not responsible for the change of mechanism since a monodentate nitrogen mustard–Pt(II) complex having a coordinated DMSO trans to the nitrogen mustard also arrested the cell cycle in the G2/M phase, shown in one of our recent publications.¹⁴ Thus, the SubG1 phase arrest is not common in similar classes of metal complexes. In addition, it is very evident that the cyclin D and Bcl-2 levels remain high in the SubG1 phase to initiate the DNA synthesis in the S-phase,^{55–57} so we also confirmed the SubG1 phase arrest by the Western blot studies. Complex **3** (Figure 8B) treated MDA-MB-231 cells showed higher contents of cyclin D and Bcl-2 compared to the untreated control, which confirm inhibition of the SubG1 phase (Figure 8D). The apoptosis initiated through intrinsic pathway leads to depolarization of the mitochondria. Complexes **1** and **3**, investigated for their ability to alter mitochondrial membrane potential, indicate that the intrinsic pathway is the major pathway of apoptosis for both of them. The change of the red fluorescence of the cationic dye JC-1 due to depolarization of mitochondria showed pronounced dose dependence especially for **3** by emitting green fluorescence at a λ_{max} of 550 nm due to the formation of JC-1 monomers (Figures 9A and S46). This is an indication that the apoptosis is mostly occurring through the intrinsic pathway. The effect is more prominent for **3** compared to **1**. In addition, the depolarization of the mitochondria leads to the release of cytochrome c, ultimately activating the effector caspases (*viz.*, caspase 3). Our studies show that both **1** and **3** activate caspase-3 in a dose-dependent fashion causing apoptosis (Figure 9B).

CONCLUSIONS

The N–O coordinated Ru(II) and Pt(II) complexes of two chloroethylamine based ligands have been synthesized, which generate a stable hydrolyzed complex at pH 7.4. These complexes bind to CT DNA with moderate affinity and form adducts with the N⁷ of the model nucleobase 9-EtG. Thus, DNA may be one of the targets for both the Ru(II) and Pt(II) complexes **1–4**. The distorted square planar Pt(II) complexes are 10–20 fold more cytotoxic than the pseudo-octahedral Ru(II) complexes of the same bidentate ligand. The toxicity of the Pt(II) complexes against pancreatic cancer (MIA PaCa-2) is ca. 30 times more than CDDP. Although both the complexes have DNA as one of their potential targets, their cell killing pathways vary since the Ru(II) complex **1** arrests the cell cycle in the G2/M phase, but the Pt(II) complex **3**, of the same

ligand (**L1**), arrests the cell cycle in the SubG1 phase. The arrest in the SubG1 phase leads to the higher expression of cyclin D and Bcl-2 by **3**. Both **1** and **3** activate caspase 3 and induce apoptotic cell death. The depolarization of the mitochondria is much higher by the Pt complex **3** than by the Ru complex **1**, suggesting the intrinsic pathway of apoptosis is favored more by **3**. Our work shows many fold higher efficacy and a change of pathway in the case of Pt(II) complexes using the same N–O coordinated bidentate ligand compared to that of the Ru(II).

ASSOCIATED CONTENT

Supporting Information

The Supporting Information is available free of charge at <https://pubs.acs.org/doi/10.1021/acs.inorgchem.0c01433>.

NMR spectra of ligands (Figures S1–S4) and complexes (Figures S5–S15), UV–vis spectra of **1–4** (Figure S16), crystal packing diagram (Figure S17), ¹H NMR and ESI-MS spectra of hydrolysis and 9-EtG binding studies of the complexes in buffer (Figures S18–S36), CT DNA binding (Figures S37 and S38), MTT assay (Figures S39–S42), and different pathways of cell killing by the complexes (Figures S43–S46) (PDF)

Accession Codes

CCDC 1992723–1992724 contain the supplementary crystallographic data for this paper. These data can be obtained free of charge via www.ccdc.cam.ac.uk/data_request/cif, or by emailing data_request@ccdc.cam.ac.uk, or by contacting The Cambridge Crystallographic Data Centre, 12 Union Road, Cambridge CB2 1EZ, UK; fax: +44 1223 336033.

AUTHOR INFORMATION

Corresponding Author

Arindam Mukherjee – Department of Chemical Sciences and Centre for Advanced Functional materials, Indian Institute of Science Education and Research Kolkata, Mohanpur 741246, West Bengal, India; orcid.org/0000-0001-9545-8628; Email: a.mukherjee@iiserkol.ac.in

Authors

Moumita Maji – Department of Chemical Sciences and Centre for Advanced Functional materials, Indian Institute of Science Education and Research Kolkata, Mohanpur 741246, West Bengal, India

Sourav Acharya – Department of Chemical Sciences and Centre for Advanced Functional materials, Indian Institute of Science Education and Research Kolkata, Mohanpur 741246, West Bengal, India; orcid.org/0000-0001-5511-1312

Saptarshi Maji – Department of Biological Sciences, Indian Institute of Science Education and Research Kolkata, Mohanpur 741246, West Bengal, India

Kallol Purkait – Department of Chemical Sciences and Centre for Advanced Functional materials, Indian Institute of Science Education and Research Kolkata, Mohanpur 741246, West Bengal, India

Arnab Gupta – Department of Biological Sciences, Indian Institute of Science Education and Research Kolkata, Mohanpur 741246, West Bengal, India

Complete contact information is available at:

<https://pubs.acs.org/10.1021/acs.inorgchem.0c01433>

Author Contributions

The manuscript was written through contributions of all authors. All authors have given approval to the final version of the manuscript.

Funding

This work was funded by SERB-DST Government of India via project number EMR/2017/002324 and ECR/2015/000220.

Notes

The authors declare no competing financial interest.

ACKNOWLEDGMENTS

We earnestly acknowledge SERB for the financial support via project number EMR/2017/002324. M.M. and S.M. thank CSIR. S.A. and K.P. thank UGC for their research fellowship. A.G. thanks Early Career Research Award from Department of Science and Technology, Govt. of India (ECR/2015/000220), and Wellcome Trust-DBT India Alliance Fellowship (IA/I/16/1/502369). All the authors sincerely thank IISER Kolkata for the financial and infrastructural support. The authors are sincerely thankful to NIBMG for the FACS facility. We also thank Mr. Tamal Ghosh for helping us in flow cytometry analysis studies.

REFERENCES

- (1) Wong, E.; Giandomenico, C. M. Current Status of Platinum-Based Antitumor Drugs. *Chem. Rev.* **1999**, *99* (9), 2451–2466.
- (2) Johnstone, T. C.; Suntharalingam, K.; Lippard, S. J. The Next Generation of Platinum Drugs: Targeted Pt(II) Agents, Nanoparticle Delivery, and Pt(IV) Prodrugs. *Chem. Rev.* **2016**, *116* (5), 3436–3486.
- (3) Wilson, J. J.; Lippard, S. J. Synthetic Methods for the Preparation of Platinum Anticancer Complexes. *Chem. Rev.* **2014**, *114* (8), 4470–4495.
- (4) Oberoi, H. S.; Nukolova, N. V.; Kabanov, A. V.; Bronich, T. K. Nanocarriers for delivery of platinum anticancer drugs. *Adv. Drug Delivery Rev.* **2013**, *65*, 1667–1685.
- (5) Chvalova, K.; Brabec, V.; Kasparkova, J. Mechanism of the formation of DNA-protein cross-links by antitumor cisplatin. *Nucleic Acids Res.* **2007**, *35* (6), 1812–1821.
- (6) Dasari, S.; Bernard Tchounwou, P. Cisplatin in cancer therapy: Molecular mechanisms of action. *Eur. J. Pharmacol.* **2014**, *740*, 364–378.
- (7) Maji, M.; Karmakar, S.; Raturaj, Gupta, A.; Mukherjee, A. Oxamuplatin: A cytotoxic Pt(II) complex of a nitrogen mustard with resistance to thiol based sequestration display enhanced selectivity towards cancer. *Dalton Trans.* **2020**, *49* (8), 2547–2558.

(8) Kenny, R. G.; Marmion, C. J. Toward Multi-Targeted Platinum and Ruthenium Drugs-A New Paradigm in Cancer Drug Treatment Regimens? *Chem. Rev.* **2019**, *119* (2), 1058–1137.

(9) Karmakar, S.; Chatterjee, S.; Purkait, K.; Mukherjee, A. Anticancer activity of a chelating nitrogen mustard bearing tetrachloridoplatinum(IV) complex: better stability yet equipotent to the Pt(II) analogue. *Dalton Trans.* **2016**, *45* (29), 11710–11722.

(10) Karmakar, S.; Purkait, K.; Chatterjee, S.; Mukherjee, A. Anticancer activity of a cis-dichloridoplatinum(II) complex of a chelating nitrogen mustard: insight into unusual guanine binding mode and low deactivation by glutathione. *Dalton Trans.* **2016**, *45* (8), 3599–3615.

(11) Karmakar, S.; Maji, M.; Mukherjee, A. Modulation of the reactivity of nitrogen mustards by metal complexation: approaches to modify their therapeutic properties. *Dalton Trans.* **2019**, *48* (4), 1144–1160.

(12) Petruzzella, E.; Braude, J. P.; Aldrich-Wright, J. R.; Gandin, V.; Gibson, D. A Quadruple-Action Platinum(IV) Prodrug with Anticancer Activity Against KRAS Mutated Cancer Cell Lines. *Angew. Chem., Int. Ed.* **2017**, *56* (38), 11539–11544.

(13) Petruzzella, E.; Sirota, R.; Solazzo, I.; Gandin, V.; Gibson, D. Triple action Pt(IV) derivatives of cisplatin: a new class of potent anticancer agents that overcome resistance. *Chem. Sci.* **2018**, *9* (18), 4299–4307.

(14) Karmakar, S.; Chatterjee, S.; Purkait, K.; Mukherjee, A. A trans-dichloridoplatinum(II) complex of a monodentate nitrogen mustard: Synthesis, stability and cytotoxicity studies. *J. Inorg. Biochem.* **2020**, *204*, 110982.

(15) Clarke, M. J.; Zhu, F.; Frasca, D. R. Non-Platinum Chemotherapeutic Metallopharmaceuticals. *Chem. Rev.* **1999**, *99* (9), 2511–2533.

(16) Tian, M.; Li, J.; Zhang, S.; Guo, L.; He, X.; Kong, D.; Zhang, H.; Liu, Z. Half-sandwich ruthenium(II) complexes containing NN-chelated imino-pyridyl ligands that are selectively toxic to cancer cells. *Chem. Commun.* **2017**, *53* (95), 12810–12813.

(17) Hartinger, C. G.; Zorbas-Seifried, S.; Jakupec, M. A.; Kynast, B.; Zorbas, H.; Keppler, B. K. From bench to bedside – preclinical and early clinical development of the anticancer agent indazolium trans-[tetrachlorobis(1H-indazole)ruthenate(III)] (KP1019 or FFC14A). *J. Inorg. Biochem.* **2006**, *100* (5–6), 891–904.

(18) Trondl, R.; Heffeter, P.; Kowol, C. R.; Jakupec, M. A.; Berger, W.; Keppler, B. K. NKP-1339, the first ruthenium-based anticancer drug on the edge to clinical application. *Chem. Sci.* **2014**, *5* (8), 2925–2932.

(19) Kuhn, P.-S.; Pichler, V.; Roller, A.; Hejl, M.; Jakupec, M. A.; Kandioller, W.; Keppler, B. K. Improved reaction conditions for the synthesis of new NKP-1339 derivatives and preliminary investigations on their anticancer potential. *Dalton Trans.* **2015**, *44* (2), 659–68.

(20) Monro, S.; Colon, K. L.; Yin, H.; Roque, J.; Konda, P.; Gujar, S.; Thummel, R. P.; Lilje, L.; Cameron, C. G.; McFarland, S. A. Transition Metal Complexes and Photodynamic Therapy from a Tumor-Centered Approach: Challenges, Opportunities, and Highlights from the Development of TLD1433. *Chem. Rev.* **2019**, *119* (2), 797–828.

(21) Meier-Menches, S. M.; Gerner, C.; Berger, W.; Hartinger, C. G.; Keppler, B. K. Structure-activity relationships for ruthenium and osmium anticancer agents - towards clinical development. *Chem. Soc. Rev.* **2018**, *47* (3), 909–928.

(22) Morris, R. E.; Aird, R. E.; del Socorro Murdoch, P.; Chen, H.; Cummings, J.; Hughes, N. D.; Parsons, S.; Parkin, A.; Boyd, G.; Jodrell, D. I.; Sadler, P. J. Inhibition of Cancer Cell Growth by Ruthenium(II) Arene Complexes. *J. Med. Chem.* **2001**, *44* (22), 3616–3621.

(23) Nowak-Sliwinska, P.; van Beijnum, J. R.; Casini, A.; Nazarov, A. A.; Wagnieres, G.; van den Bergh, H.; Dyson, P. J.; Griffioen, A. W. Organometallic Ruthenium(II) Arene Compounds with Antiangiogenic Activity. *J. Med. Chem.* **2011**, *54* (11), 3895–3902.

(24) Ronconi, L.; Sadler, P. J. Using coordination chemistry to design new medicines. *Coord. Chem. Rev.* **2007**, *251*, 1633–1648.

- (25) Romero-Canelon, I.; Salassa, L.; Sadler, P. J. The Contrasting Activity of Iodido versus Chlorido Ruthenium and Osmium Arene Azo- and Imino-pyridine Anticancer Complexes: Control of Cell Selectivity, Cross-Resistance, p53 Dependence, and Apoptosis Pathway. *J. Med. Chem.* **2013**, *56* (3), 1291–1300.
- (26) Pantic, D. N.; Arandelovic, S.; Radulovic, S.; Roller, A.; Arion, V. B.; Grguric-Sipka, S. Synthesis, characterisation and cytotoxic activity of organoruthenium(II)-halido complexes with 1H-benzimidazole-2-carboxylic acid. *J. Organomet. Chem.* **2016**, *819*, 61–68.
- (27) Ware, D. C.; Palmer, B. D.; Wilson, W. R.; Denny, W. A. Hypoxia-selective antitumor agents. 7. Metal complexes of aliphatic mustards as a new class of hypoxia-selective cytotoxins. Synthesis and evaluation of cobalt(III) complexes of bidentate mustards. *J. Med. Chem.* **1993**, *36* (13), 1839–46.
- (28) Parker, L. L.; Lacy, S. M.; Farrugia, L. J.; Evans, C.; Robins, D. J.; O'Hare, C. C.; Hartley, J. A.; Jaffar, M.; Stratford, I. J. A Novel Design Strategy for Stable Metal Complexes of Nitrogen Mustards as Bioreductive Prodrugs. *J. Med. Chem.* **2004**, *47* (23), 5683–5689.
- (29) Khokhar, A. R.; Xu, Q.; Newman, R. A.; Kido, Y.; Siddik, Z. H. Synthesis, characterization, and antitumor activity of new chloroethylamine platinum complexes. *J. Inorg. Biochem.* **1992**, *45* (3), 211–19.
- (30) Rahman, F.-U.; Ali, A.; Duong, H.-Q.; Khan, I. U.; Bhatti, M. Z.; Li, Z.-T.; Wang, H.; Zhang, D.-W. ONS-donor ligand based Pt(II) complexes display extremely high anticancer potency through autophagic cell death pathway. *Eur. J. Med. Chem.* **2019**, *164*, 546–561.
- (31) Puttock, E. V.; Fradgley, J. D.; Yufit, D. S.; Williams, J. A. G. A family of readily synthesised phosphorescent platinum(II) complexes based on tridentate NNO-coordinating Schiff-base ligands. *Dalton Trans.* **2019**, *48* (40), 15012–15028.
- (32) Bandeira, S.; Gonzalez-Garcia, J.; Pensa, E.; Albrecht, T.; Vilar, R. A Redox-Activated G-Quadruplex DNA Binder Based on a Platinum(IV)-Salphen Complex. *Angew. Chem., Int. Ed.* **2018**, *57* (1), 310–313.
- (33) Acharya, S.; Maji, M.; Rutaraj; Purkait, K.; Gupta, A.; Mukherjee, A. Synthesis, Structure, Stability, and Inhibition of Tubulin Polymerization by Ru(II)-p-Cymene Complexes of Trime-thoxyaniline-Based Schiff Bases. *Inorg. Chem.* **2019**, *58* (14), 9213–9224.
- (34) Cassells, I.; Stringer, T.; Hutton, A. T.; Prince, S.; Smith, G. S. Impact of various lipophilic substituents on ruthenium(II), rhodium(III) and iridium(III) salicylaldehyde-based complexes: synthesis, in vitro cytotoxicity studies and DNA interactions. *JBIC, J. Biol. Inorg. Chem.* **2018**, *23* (5), 763–774.
- (35) Ding, F.; Sun, Y.-g.; Verpoort, F.; Dragutan, V.; Dragutan, I. Catalytic activity and selectivity of a range of ruthenium complexes tested in the styrene/EDA reaction system. *J. Mol. Catal. A: Chem.* **2014**, *386*, 86–94.
- (36) Gatti, A.; Habtemariam, A.; Romero-Canelon, I.; Song, J.-I.; Heer, B.; Clarkson, G. J.; Rogolino, D.; Sadler, P. J.; Carcelli, M. Half-Sandwich Arene Ruthenium(II) and Osmium(II) Thiosemicarbazone Complexes: Solution Behavior and Antiproliferative Activity. *Organometallics* **2018**, *37* (6), 891–899.
- (37) Du, Q.; Guo, L.; Tian, M.; Ge, X.; Yang, Y.; Jian, X.; Xu, Z.; Tian, Z.; Liu, Z. Potent Half-Sandwich Iridium(III) and Ruthenium(II) Anticancer Complexes Containing a P⁺O-Chelated Ligand. *Organometallics* **2018**, *37* (17), 2880–2889.
- (38) Li, J.; Tian, M.; Tian, Z.; Zhang, S.; Yan, C.; Shao, C.; Liu, Z. Half-Sandwich Iridium(III) and Ruthenium(II) Complexes Containing P-P-Chelating Ligands: A New Class of Potent Anticancer Agents with Unusual Redox Features. *Inorg. Chem.* **2018**, *57* (4), 1705–1716.
- (39) Li, J.; Tian, Z.; Xu, Z.; Zhang, S.; Feng, Y.; Zhang, L.; Liu, Z. Highly potent half-sandwich iridium and ruthenium complexes as lysosome-targeted imaging and anticancer agents. *Dalton Trans.* **2018**, *47* (44), 15772–15782.
- (40) Bennett, M.; Huang, T. N.; Matheson, T.; Smith, A.; Ittel, S.; Nickerson, W. (η^6 -Hexamethylbenzene) ruthenium Complexes. *Inorg. Synth.* **2007**, *21*, 74–78.
- (41) Kukushkin, V.; Pombeiro, A.; Ferreira, C.; Elding, L. Dimethylsulfoxide Complexes of Platinum(II): K[PtCl₃(Me₂SO)], cis-[PtCl₂L(Me₂SO)] (L = Me₂SO, MeCN), [PtCl(μ -Cl)-(Me₂SO)]₂, and [Pt(Me₂SO)₄](CF₃SO₃)₂. *Inorg. Synth.* **2002**, *33*, 189–196.
- (42) Grivani, G.; Vakili, M.; Khalaji, A. D.; Bruno, G.; Rudbari, H. A.; Taghavi, M.; Tahmasebi, V. Synthesis, characterization, crystal structure determination, computational study, and thermal decomposition into NiO nano-particles of a new Ni(II) Schiff base complex (L = 2-(E)-[(2-chloroethyl)imino]methylphenolate). *J. Mol. Struct.* **2014**, *1072*, 77–83.
- (43) Dolomanov, O. V.; Bourhis, L. J.; Gildea, R. J.; Howard, J. A. K.; Puschmann, H. OLEX2: a complete structure solution, refinement and analysis program. *J. Appl. Crystallogr.* **2009**, *42* (2), 339–341.
- (44) Sheldrick, G. A short history of SHELX. *Acta Crystallogr., Sect. A: Found. Crystallogr.* **2008**, *64* (1), 112–122.
- (45) Sheldrick, G. SHELXT - Integrated space-group and crystal-structure determination. *Acta Crystallogr., Sect. A: Found. Adv.* **2015**, *71* (1), 3–8.
- (46) Sheldrick, G. Crystal structure refinement with SHELXL. *Acta Crystallogr., Sect. C: Struct. Chem.* **2015**, *71* (1), 3–8.
- (47) Marmur, J. A procedure for the isolation of deoxyribonucleic acid from microorganisms. *J. Mol. Biol.* **1961**, *3*, 208–18.
- (48) Grivani, G.; Tahmasebi, V.; Khalaji, A. D.; Fejfarova, K.; Dusek, M. Synthesis, characterization and crystal structure determination of a new vanadium(IV) Schiff base complex (VOL2) and investigation of its catalytic activity in the epoxidation of cyclooctene. *Polyhedron* **2013**, *51*, 54–60.
- (49) Backler, F.; Wilson, G. J.; Wang, F. Rational use of ligand to shift the UV-vis spectrum of Ru-complex sensitizer dyes for DSSC applications. *Radiat. Phys. Chem.* **2019**, *161*, 66–71.
- (50) Kumar, K. N.; Venkatachalam, G.; Ramesh, R.; Liu, Y. Half-sandwich para-cymene ruthenium(II) naphthylazophenolato complexes: Synthesis, molecular structure, light emission, redox behavior and catalytic oxidation properties. *Polyhedron* **2008**, *27* (1), 157–166.
- (51) Kubanik, M.; Holtkamp, H.; Sohnel, T.; Jamieson, S. M. F.; Hartinger, C. G. Impact of the Halogen Substitution Pattern on the Biological Activity of Organoruthenium 8-Hydroxyquinoline Anticancer Agents. *Organometallics* **2015**, *34* (23), 5658–5668.
- (52) Sitati, M. K.; Jaganyi, D.; Mambanda, A., The rate of substitution from η^6 -arene ruthenium(II) complexes. *Transition Met. Chem.* **2020** [Ahead of Print], DOI: 10.1007/s11243-020-00380-1.
- (53) Chow, M. J.; Babak, M. V.; Wong, D. Y. Q.; Pastorin, G.; Gaiddon, C.; Ang, W. H. Structural Determinants of p53-Independence in Anticancer Ruthenium-Arene Schiff-Base Complexes. *Mol. Pharmaceutics* **2016**, *13* (7), 2543–2554.
- (54) Ghose, A. K.; Viswanadhan, V. N.; Wendoloski, J. J. A Knowledge-Based Approach in Designing Combinatorial or Medicinal Chemistry Libraries for Drug Discovery. 1. A Qualitative and Quantitative Characterization of Known Drug Databases. *J. Comb. Chem.* **1999**, *1* (1), 55–68.
- (55) Zinkel, S.; Gross, A.; Yang, E. BCL2 family in DNA damage and cell cycle control. *Cell Death Differ.* **2006**, *13* (8), 1351–1359.
- (56) Gao, G.; Dou, Q. P. G1 phase-dependent expression of Bcl-2 mRNA and protein correlates with chemoresistance of human cancer cells. *Mol. Pharmacol.* **2000**, *58* (5), 1001–1010.
- (57) Yang, K.; Hitomi, M.; Stacey, D. W. Variations in cyclin D1 levels through the cell cycle determine the proliferative fate of a cell. *Cell Div.* **2006**, *1*, 32.